Maximizing Wireless Power Transfer Using Ferrite Rods within Telemetric Devices for Rodents

Basem M. Badr[1], Robert Somogyi-Csizmazia[2], Kerry R. Delaney[2], and Nikolai Dechev[1]

[1]Department of Mechanical Engineering, University of Victoria, Victoria, BC, Canada, [2]Department of Biology, University of Victoria, Victoria, BC, Canada.
*Corresponding author: 3800 Finnerty Road, Victoria, BC, V8W 2Y2, bbadr@uvic.ca

Abstract: A number of medical and research applications require implantable devices to locally stimulate internal organs and communicate the internal vital signals to the outer world. Wireless power transfer (WPT) technique is used to supply power to these devices. The power is transferred wirelessly from a stationary primary coil to a movable secondary coil. The secondary device is implanted in a rodent, which moves freely inside a cage around which the primary is wrapped. However, the continuously changing orientation of the rodent leads to coupling loss/problems between the primary and secondary coils. We propose configurations of the secondary coil employing different size of ferrite rods placed at specific locations within the coil. Three dimensional finite element analysis (FEA) using COMSOL software, is used to find the magnetic flux density distribution surrounding these secondary configurations. The simulation results show a significant increase of flux through the coil using the ferrite arrangement, with improved coupling at most orientations. The secondary coil configurations were constructed and experiments were conducted to test their performance. Measurements show that ferrite rods improved power transfer, where the long ferrite (4LF) configuration is highest received power. Experiments show the maximum power collected by 4LF was 127 mW when parallel to the primary coil.

Keywords: Wireless power transfer, Magnetic resonance, Biomedical device, Finite element analysis, Implants.

1. Introduction

Implantable biomedical telemetry devices have gained much attention for a variety of applications including generating stimulus signals, monitoring the body, and communicating internal vital signs to the outer world. Providing power to these devices for long term is a challenging task [1]. Traditionally, implantable batteries and percutaneous link power supply systems are used. However, the batteries have limited energy storage and life span, and the percutaneous links across the skin impose infection risks [2]. For applications involving rodents, battery size and weight is more problematic for long duration experiments (1 or more days). In some cases, implants use rechargeable batteries, where those systems employ wireless recharging [1].

The use of animal models for human disease processes plays a vital role in biomedical research. A vast majority of the research on neural mechanisms of therapies is currently conducted using rodent models. Implantable biotelemetry systems are effective tools for clinical medicine and also in animal research, because they allow for the acquisition of otherwise unavailable physiological data [1]. Rodents are important animals used for biomedical applications, and are widely used to study various disease models [3]. When studying the behavior of rodents and gathering biological data from them, miniature sensors and telemetry devices are needed. These devices must provide continuous monitoring without limiting rodents mobility or behavior. This work motivates to power these sensors and devices.

This work proposes the use of a wireless power transfer (WPT) system to continuously power a rodent telemetric device. It was found that a number of researchers are investigating WPT for rodents, as mentioned in [1, 4]. The proposed application is for a rodent implant device (RID) that can act as a stimulator and sensor, for a freely moving small rodent. The current RID prototype is suitable for subcutaneous implantation in a rat, and is suitable as a head-

mounted device for a mouse. Figure 1 illustrates the mouse-based concept for telemetry acquisition, where the telemetric device is located on the head of a freely moving mouse. The mouse moves within a stationary primary coil wrapped around a small mouse housing cage sized 250 × 120 × 150 mm (length × width × height). This cage size is needed to meet the minimum animal care standards for mice.

A common characteristic of WPT applications for rodent telemetry acquisition is loose coupling between the primary and secondary coils. The coupling coefficient of loosely coupled WPT (LCWPT) systems is between 1-10%, which greatly limits power transfer [1, 4-5]. To compensate for loose coupling, the use of magnetic resonant systems is employed, to create boosted voltage/current levels at the secondary coil and minimize the losses at the primary section [1]. Such resonant power transfer is dependent on factors such as the frequency match between the inherent resonant frequency of the primary circuit, and the inherent resonant frequency of the secondary circuit [1, 4].

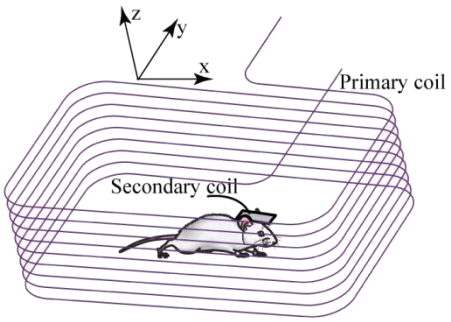

Figure 1. Small Rodent WPT concept.

The LCWPT systems have restrictions on the loop diameters of the secondary coils, the weight of the implanted/mounted devices, and the separation of the primary coil and the secondary coil. The secondary coil exhibits low coupling with the primary coil when the *air core* coil plane is at high orientations [1, 4]. For our rodent telemetry application (RID), as illustrated in Fig. 1, the rodent moves freely within the cage. Hence, its orientation is constantly changing, which results in variable coupling. Therefore, the main focus of this paper is improving the mutual inductance (coupling coefficient) between the primary and secondary coils, by inserting ferrite rods located at specific locations within the secondary coil. To show the effect of using ferrites, four configurations are used in this work, which are called the *air core*, 4SF (short ferrite), 4MF (medium ferrite) and 4LF (long ferrite) configurations. The three configurations use the same diameter (1.6 mm) of ferrite rods and with different ferrite length.

This paper is organized as follows. Section I provides the research motivation for the proposed WPT system. Section II describes WPT theory. Section III describes the simulation work done using finite element analysis (FEA) with COMSOL software. Experimental works are presented and discussed in Section IV. Finally, the conclusion is in Section V.

2. WPT Theory

Electromagnetic inductive power transfer (IPT) is a popular technique for WPT over a near field coupling. This technique is based on two fundamental laws: Ampere's law and Faraday's law. IPT is based on the changing magnetic field that is created due to alternating currents through a primary coil that induce a voltage onto a secondary coil [1]. The current flows through the primary coil, a magnetic field (H) and a corresponding magnetic flux (φ) are generated. The secondary coil captures a portion of the flux generated by the primary coil, a mutual inductance results that can be denoted as [6]:

$$M_{SP} = \frac{\Psi_{SP}}{I_P} \tag{1}$$

where I_P is the current applied to the primary coil, and ψ_{SP} is the total flux captured by the secondary coil due to the current I_P flowing through the primary coil. The total capture flux by the secondary coil can be written as [6]:

$$\Psi_{SP} = \mu_0 \times H(I_P) \times N_S \times A_S \tag{2}$$

where, $H(I_P)$ are the flux density and magnetic field strength due to the applying primary current I_P, μ_0 is the permeability of free space, and A_S is the area enclosed by secondary coil. The resulting magnetic field strength at the secondary

coil can be obtained by integrating Biot-Savart's law around the primary coil [1]:

$$H = \frac{I_P N_P {r_P}^2}{2(\sqrt{{r_P}^2 + r^2})^3} \quad (3)$$

where, N_P is the number of primary turns, r is the transmission distance, and r_P is the primary coil radius. The mutual inductance of *air core* can be obtained by combining the equations (1, 2 and 3), it is given as:

$$M_{SP} = \frac{\mu_0 N_P {r_P}^2 N_S {r_S}^2 \pi}{2(\sqrt{{r_P}^2 + r^2})^3} \quad (4)$$

where r_s is the radius of the secondary coil. When the coils are merely angularly misaligned the approximation mutual inductance ($M_{SP} \times cos\theta$) can be applied, where θ is the angle between the axis of the two coils. When a ferromagnetic material is inserted within the coils, the mutual inductance increases due to an increase in permeability and thus an enhancement of the magnetic flux through the secondary coil. The aim of using ferrite rods in inductively coupled systems is to improve the power transfer between the primary and secondary coils.

The best ferrite utilization occurs when the ferrite rods are made as long as possible. The gradient of the ferrite length curve is the highest which is as expected since longer rods permit the longest flux paths in air above each bar [1, 7]. The magnetic flux is not constant throughout the volume of the ferrite rod, as the ferrite rods are cylindrical in shape. The maximum pulling magnetic flux occurs at the center of the rod, however, the magnetic flux reaches to the minimum at the ends [1, 6]. The magnetic flux density at the center of the ferrite rod is given as [6]:

$$B_c = \frac{\mu_0 \mu_r H_c}{1 + D_f(\mu_r - 1)} \quad (5)$$

where, H_C is the magnetic field strength at the center of the ferrite rod, D_f is a demagnetizing factor, it can be defined as [6]:

$$D_f = -\frac{\mu_0 H_D}{J_C} \quad (6)$$

where, J_C is the magnetic polarization of the ferrite at the center, H_D is the magnetizing field. The mutual inductance was calculated for the case of the radius of the ferrite rod (r_f) is less than the radius of the secondary coil (r_s), and the length of the ferrite rod (l_f) is higher than the length of the secondary coil (l_s). The mutual inductance of this configuration is approximated as [6]:

$$M_{SP} = \frac{\mu_0 N_P {r_P}^2 N_S {r_S}^2 \pi}{2(\sqrt{{r_P}^2 + r^2})^3} \left[\left[1 - \frac{{r_f}^2}{{r_s}^2}\right] + \sqrt[3]{\frac{l_f}{l_s}} \frac{\mu_r}{1 + D_{fc}(\mu_r - 1)} \left[\frac{{r_f}^2}{{r_s}^2}\right]\right] \quad (7)$$

where, D_{fc} is the cylindrical demagnetizing factor, it is calculated as [6]:

$$D_{fc} = D_{fe}(0.755\gamma^{0.13}) \quad (8)$$

$$D_{fe} = \frac{{r_f}^2}{\frac{l_f}{2(r_f)^2 e^3}} \left[\ln\left(\frac{1+e}{1-e}\right) - 2e\right] \quad (9)$$

$$e = \sqrt{1 - \left(\frac{2r_f}{l_f}\right)^2} \quad (10)$$

where, γ is the ratio of the length to diameter.

3. Use of COMSOL Multiphysics

A simulation using 3-D FEA with COMSOL software is done to determine the magnetic field distribution surrounding the various secondary configurations. COMSOL is used to understand how the primary magnetic field interacts with the ferrite rods in the secondary coil, when the secondary is oriented with respect to the primary field. Also, to correlate the total flux captured by the secondary coil to the ferrite rod size and location within the secondary. A Frequency Domain Study is used to investigate the WPT model at an applied frequency, corresponding to the system's resonant frequency. A simulated current of 2.5 A (peak-to-peak) is applied through the primary coil windings. The secondary coil is modeled as a simplified one wire loop. The simulations are done for the 4SF, 4MF and 4LF configurations, these configurations use four pieces of ferrite rod (FR) placed within the corners of the secondary air core coil (SC), as shown in Figure 2. The 4SF, 4MF and 4LF configurations have same diameter (1.6 mm) of the ferrite rods, but have different length that are 3.2 mm, 6.4 mm and 10 mm

respectively. The type of ferrite rod used in this work is 4B1, which is suitable for the operating frequency of our WPT system. Its material specifications [8] are configured in COMSOL, including the B-H curve and permeability as a function of frequency.

The parts of each configuration are meshed using different elements, with different mesh settings. The sphere domain and the ferrite rods are modeled with tetrahedral elements, using the Finer and the Extremely Fine meshing settings, respectively. Figure 2 illustrates the meshing of the four configurations. The internal COMSOL mesh quality was found to be of high quality.

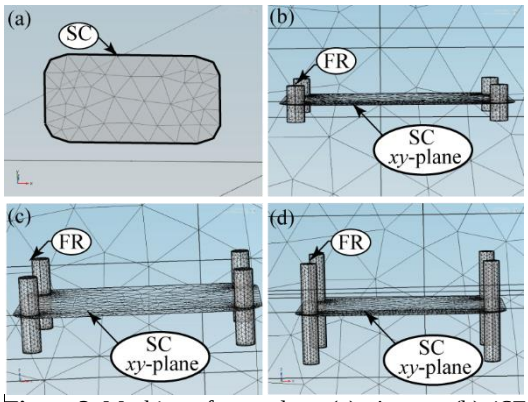

Figure 2. Meshing of secondary: (a) *air core*, (b) 4SF, (c) 4MF and (d) 4LF.

The magnetic field is locally attracted by the ferrite, which improves the coupling between the primary and secondary coils. Figure 3 shows an *x-y* plane plot of the magnetic flux density distribution produced by the primary coil, at the middle of the cage. Note line AB shown in Figure 3 (b, c and d), which passes through two ferrites on the *x-y* plane, is used to plot the magnetic flux density. The magnitude of the flux density crossing the secondary coil, along line AB is then determined, and is plotted in Figure 4. Using the plotted information of Figure 4, the total flux ψ_{SP} passing perpendicularly through the inside of the secondary coil *x-y* plane is computed, as listed in Table 1.

4. Experimental Works

The four configurations have been physically prototyped and are tested using our designed WPT system. Figure 5 shows schematic diagram of our WPT system that can be divided into two parts, namely the primary and secondary sections. The parallel-parallel (PP) configuration is used to achieve magnetic resonance between primary and secondary sections. The magnetic resonant coupling is accomplished by tuning the primary section such that both sections resonate at the same frequency.

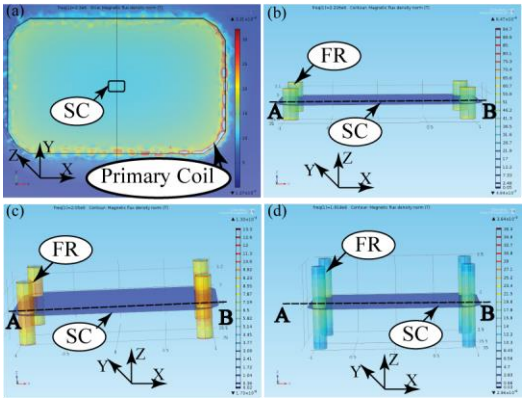

Figure 3. Plot of the magnetic flux density: (a) plotted on the *x-y* plane within and around the primary coil, (b) 4SF, (c) 4MF and (d) 4LF configuration.

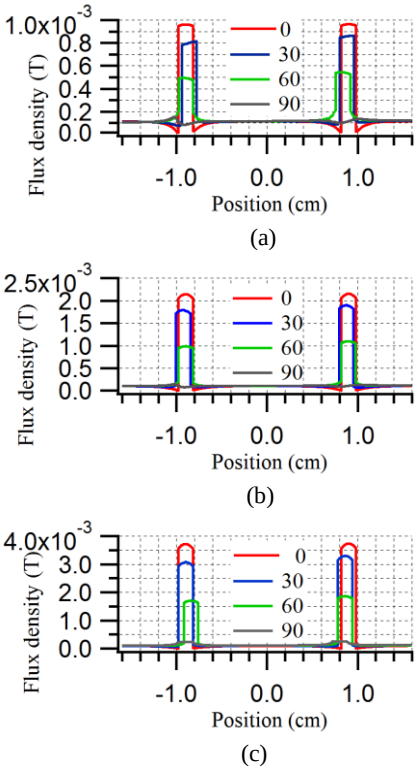

Figure 4. Waterfall plot of the magnetic flux density within the ferrite rods and the air space around them; (a) 4SF, (b) 4MF and (c) 4LF.

Table 1: Simulation results of secondary coil configurations

Configuration	Flux through Coil $(Wb) \times 10^{-8}$	Flux Density in Ferrite (Wb/m^2)	Total Flux ψ_{SP} in Config $(Wb) \times 10^{-8}$
Air core, 0˚	2.95	0	2.95
Air core, 30˚	2.56	0	2.56
Air core, 60˚	1.48	0	1.48
Air core, 90˚	0	0	0
4SF, 0˚	2.37	1.15E-03	3.29
4SF, 30˚	2.32	8E-04	2.84
4SF, 60˚	1.61	3.5E-04	1.89
4SF, 90˚	0	6E-5	0.048
4MF, 0˚	2.37	2.20E-03	4.14
4MF, 30˚	2.32	1.60E-03	3.61
4MF, 60˚	1.61	7E-04	2.17
4MF, 90˚	0	1.5E-4	0.12
4LF, 0˚	2.37	3.70E-03	5.34
4LF, 30˚	2.32	2.80E-03	4.58
4LF, 60˚	1.61	1.90E-03	3.14
4LF, 90˚	0	1.90E-04	0.153

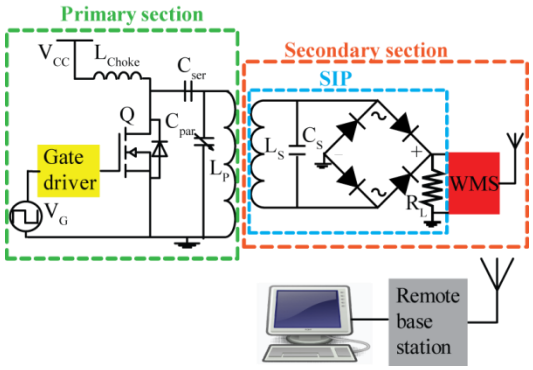

Figure 5. Schematic diagram of proposed WPT.

A Class-E power amplifier is designed to convert the DC supply to AC sinusoidal voltage and current. The AC sinusoidal current (I_P) is applied to the primary coil (L_P), and generates an oscillating electromagnetic field. The alternating electromagnetic field induces a sinusoidal voltage in the secondary coil (L_S) of the secondary implant prototype (SIP). The induced DC voltage is measured across the load (R_L), using a custom wireless measurement system (WMS) that we have designed. The WMS is powered by battery and communicates via radio to a remote base station connected to a laptop. The WMS helps our WPT measurements, since it overcomes many problems when using oscilloscope probes, to measure the induced voltage of the secondary circuit [1].

A pulse train (V_G, duty cycle 0.5) is applied at the NMOSFET gate. The C_{par} preserves the switch from high current amplitudes, and C_{ser} shields the switch MOSFET from the high voltage over the primary L_P. The choke inductor L_{choke} blocks the ac current from the supply [9]. The parallel capacitance normally present in a Class-E amplifier has been replaced here by a diode where the diode allows for suboptimum operation meets the power specifications [1].

The SIP consists of a LC-tank (different for each of the four configurations) and a full bridge rectifier. The used resonant capacitor (C_S) is 235 pF for the four configurations. Figure 6 shows the cross section of the *air core*, 4SF, 4MF and 4LF configurations. All four configurations of the secondary coil employ 48 AWG Litz wire, where the number of turns used is 28 turns. The secondary coil (L_S) was wrapped around a PCB, the dimension the PCB is 20.25×13.25×2 mm (length×width×height).

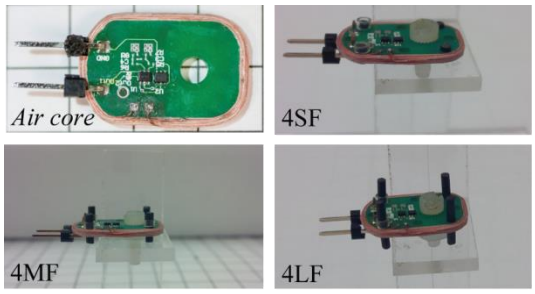

Figure 6. SIP of *air core*, 4SF, 4MF and 4LF.

A working prototype of the WPT system has been built, which employs a primary coil wrapped around an animal cage of 250×120×150 mm (length × width × high) in size. To mimic the orientation of a mouse, four experimental fixtures were constructed to hold the SIP at various orientations, to test WPT coupling. These orientations are 0°, 30°, 60° and 90°, with respect to the *x*–*y* plane. Figure 7 shows the experimental setup of the WPT system, as well as the fixtures used for the orientations. Table 2 shows the parameters of the secondary coils, which are measured by LCR meter. The measured resonant frequencies of the *air core*, 4SF, 4MF and 4LF configurations are 2.3, 2.22, 2.05 and 1.92 MHz, respectively.

Table 2: Parameters of the secondary coils

Configuration	Q	L (μH)
Air core	36	22.4
4SF	41	25.2
4MF	44	29.5
4LF	48	34.3

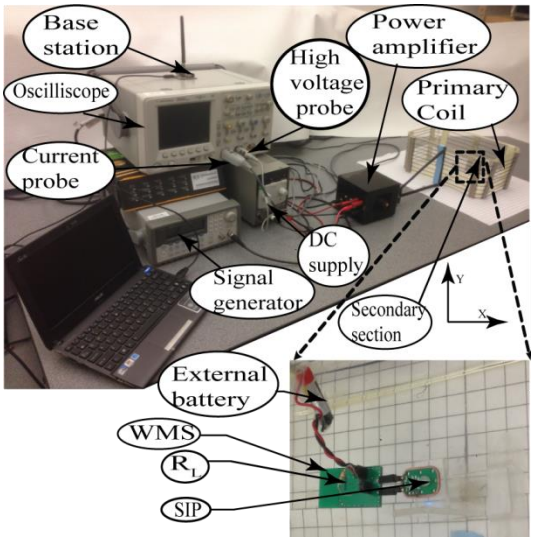

Figure 7. Experimental setup of WPT.

A series of applied sinusoidal currents (I_P) are supplied to the primary, with values of: 1, 1.5, 2 and 2.5 A (peak-to-peak). The resulting power induced in the secondary is measured and recorded. Figure 8 shows the power transferred to the *air core* configuration at the middle of the cage with different orientations. The *air core* uses a R_L value of 5 kΩ, to achieve impedance matching within the SIP. The maximum power received of *air core* configuration is 58 mW, which occurs at the 0° orientation with a primary coil current (I_P) of 2.5 A.

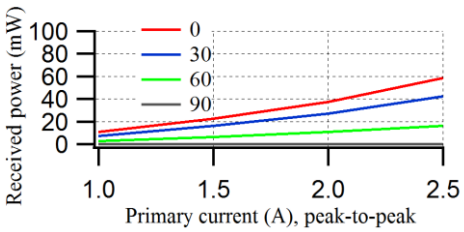

Figure 8. Power received of *air core* configuration with a 5 KΩ load R_L.

Figure 9 shows a plot of the power transferred to the 4SF configuration at the middle of the primary cage. 4SF uses a R_L value of 5 kΩ to achieve impedance matching within the SIP. The maximum power received of 4SF is 67 mW. Figure 10 shows a plot of the power transferred to the 4MF configuration at the middle of the primary cage. The 4MF configuration uses a R_L value of 10 kΩ to achieve impedance matching within the SIP. The maximum power received of 4MF is 86 mW. Figure 11 shows a plot of the power transferred to the 4LF configuration at the middle of the primary cage. The 4LF configuration uses a R_L value of 10 kΩ to achieve impedance matching within the SIP. The maximum power received of 4LF is 127 mW.

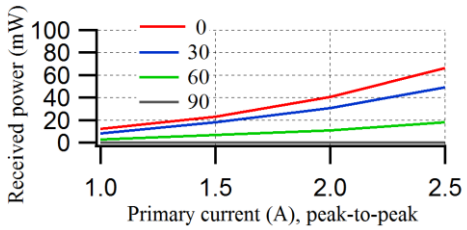

Figure 9. Power received of 4SF configuration with a 5 KΩ load R_L.

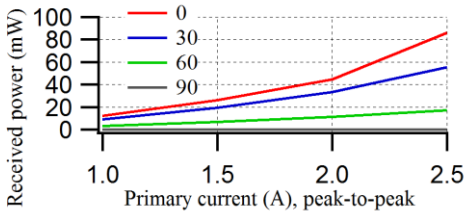

Figure 10. Power received of 4MF configuration with a 10 KΩ load R_L.

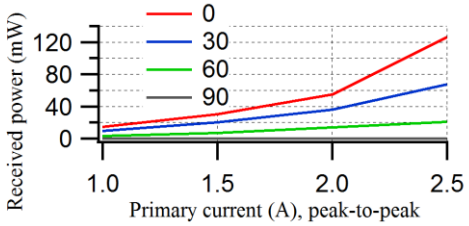

Figure 11. Power received of 4LF configuration with a 10 KΩ load R_L.

The results of Figures 8-11 are expected and match the theory. The induced voltage (V_{ind}) of the four configurations with applying 2.5 A, are recorded in Table 3. The ability of the *air core* coil to harvest magnetic flux is directly proportional to the coil area through which the

primary field passes, which defines the induced voltage (V_{ind}) in the secondary coil. Addition of ferrites draws more flux into the coil, resulting in improved coupling and hence power transfer.

Some comparisons can be made between the simulation results and the experimental results, in relation to induced voltage improvements from the addition of ferrite rods. Note that the simulation results are non-resonant [1], while the experimental results are resonant, hence, only comparisons of normalized trends can be made. Table 3 shows the total flux ψ_{SP} calculated from the simulation results (from Table 1), and the induced voltage (V_{ind}) measured from experiment. Also included is the normalized percent variation (NPV), defined as: $\psi_{SP}/(\psi_{SP}$ at 0°), and $V_{ind}/(V_{ind}$ at 0°) for simulation and experiment, respectively. It can be seen that the NPV for the simulation matches the NPV for the experiment quite well.

Table 3: Comparison between simulation and experimental results of secondary coil configurations

	Simulation		Experiment	
	Total Flux ψ_{SP}	NPV	Induced Voltage	NPV
Configuration	($Wb \times 10^{-8}$	(%)	(V_{ind})	(%)
Air Core, 0˚	2.95	100	17.1	100
Air Core, 30˚	2.56	87	14.6	85
Air Core, 60˚	1.48	50	9.1	53
Air Core, 90˚	0	0	0.14	1
4SF, 0˚	3.29	100	18.2	100
4SF, 30˚	2.84	86.3	15.7	86.17
4SF, 60˚	1.89	57.4	9.4	51.78
4SF, 90˚	0	1.47	0.18	1.00
4MF, 0˚	4.14	100	29.36	100
4MF, 30˚	3.61	87.2	23.49	80.1
4MF, 60˚	2.17	52.5	13.1	44.7
4MF, 90˚	0	2.9	0.3	1.08
4LF, 0˚	5.34	100	35.6	100
4LF, 30˚	4.58	85.6	29.15	81.8
4LF, 60˚	3.14	58.7	18.7	52.5
4LF, 90˚	0.153	2.8	0.89	2.5

5. Conclusions

This paper has investigated a WPT system suitable for transmitting power to a telemetric device located on a freely moving rodent. Using ferrite rods placed within the secondary coil improves the coupling coefficient, so the power transfer increases. FEA simulation finds the longer the ferrite rods pulls more flux, as the most attraction flux is done by 4LF configuration. The 4LF configuration was shown to provide up to 127 mW of power when oriented at 0° to the primary field. For any WPT system, some form of application circuit will reside on a PCB to perform a function. In such a case, the secondary coil winding can be wrapped around the perimeter of the PCB, with four ferrites to be placed in the corners inside the coil.

9. References

[1] B. M. Badr, R. Somogyi-Gsizmazia, K. R. Delaney and N. Dechev, Wireless Power Transfer for Telemetric Devices with Variable Orientation, for Small Rodent Behavior Monitoring, *IEEE Sensor Journal*, **15**, pp. 2144-2156, April, 2015.

[2] P. Si, A. P. Hu, J. W. Hsu, M. Chiang, Y. Wang, S. Malpas, and D. Budgett, Wireless Power Supply for Implantable Biomedical Device Based on Primary Input Voltage Regulation, *IEEE Industrial Electronics and Applications Conference*, Harbin, China, May 23–25, 2007.

[3] P. Wouters, R. Puers, R. Geers, and V. Goedseels, Implantable Biotelemetry Devices for Animal Monitoring and Identification, *IEEE EMBS Conf.*, pp. 2665–2666, Paris, France, Oct. 29–Nov. 1, 1992.

[4] B. M. Badr, R. Somogyi-Gsizmazia, N. Dechev and K. R. Delaney, Power Transfer via Magnetic Resonant Coupling for Implantable Mice Telemetry Device, *IEEE WPTC*, pp. 259–264, Jeju, South Korea, May 8–9, 2014.

[5] Z. Yang, W. Liu, and E. Basham, Inductor Modeling in Wireless Links for Implantable Electronics, *IEEE Trans. Magn.*, **43**, pp. 3815-3860, Sep., 2007.

[6] P. T. Theilmann, and P. M. Asbeck, An Analytical Model for Inductively Coupled Implantable Biomedical Devices with Ferrite Rods, *IEEE Trans. Biomed. Circuits Syst.*, **3**, pp. 43-52, Feb., 2009.

[7] M. Budhia, G. A. Covic, and J. T. Boys, "Design and Optimisation of Magnetic Structures for Lumped Inductive Power Transfer Systems, *IEEE ECCE Conf.*, pp. 2081–2088, San Jose, USA, Sep. 20–24, 2009.

[8] Ferrite 4B1. (2014, Oct 15). [Online]. Available: http://www.ferroxcube.com.

[9] B. Lenaerts, and R. Puers, An Inductive Power Link for a Wireless Endoscope, *Journal of Biosensors and Bioelectronics*, vol. 22, no. 7, pp. 1390-1395, Feb., 2007.